SHADOW DETECTION FROM MULTIBAND IMAGER VIA CONDITIONAL GENERATIVE ADVERSARIAL NETWORK. R. Ito[1], H. Inoue[2], M. Ohtake[2], Y. Ishihara[2], H. Ootake[2], R Nakamura[1] [1]National Institute of Advanced Industrial Science and Technology/Artificial Intelligence Research Center, 2-4-7 Aomi, Koto-ku, Tokyo 135-0064, Japan (pscrh.itou@aist.go.jp); [2] Japan Aerospace Exploration Agency/Institute of Space and Astronautical, 3-1-1 Yoshinodai, Sagamihara-shi, Kanagawa 252-5210, Japan.

Introduction: Low reflectance regions, known as dark mantle deposits (DMD), exist on the lunar surface, and it is very important to examine the global distribution. While smaller DMDs can be located based on the accumulating high resolution lunar images, the automatic determination of small DMDs may be hindered by the shadows in Kaguya's Multiband Imager (MI) images [1]. This study aims to enable the detection of smaller DMDs on the global lunar surface using the MI images with masked shadow regions. A method for the detection of shadow regions prior to the locating of the DMDs is considered herein.

Initially, we performed a simulation of solar illumination using the SLDEM [2] data corresponding to an MI image. Many dark regions that appear as shadows exist in the MI image; however, shaded (sunless) regions are almost entirely absent in the simulation results. This suggests that the regions that appear as shadows are not the actual shadows cast by being hidden from sunshine but are rather areas that have a relatively low reflectance compared to the surrounding area owing to the difference in the local solar incidence angle. However, these regions often exhibit abnormal spectrum patterns. Therefore, the regions that appear to be shadows should be excluded from DMD candidates. In this study, these regions are treated in a similar manner as the actual shadows.

For detecting the shadows on the pixel basis, the shadows should be directly detected from the MI images. Generative Adversarial Network (GAN) is a deep learning method recently used for style transfer, segmentation, or super resolution in the field of computer vision. The GAN comprises two networks: the Generator and Discriminator. The Generator is trained to generate realistic fake images that cannot be distinguished from real images by the Discriminator, whereas the Discriminator is trained to detect the fake images generated by the Generator.The conditional GAN (cGAN) [2] is used for detecting shadows herein. The ability to control the output image of the Generator by adding an observed image to the input data of the networks is an advantage of cGAN. The Generator of normal GAN learns a mapping from the random noise vector, and the Discriminator learns from a either real or fake images. Conversely, the Generator of cGAN learns a mapping from the observed images and the random noise vector, and the Discriminator learns from the pairs of observed image and either real or fake images.

Method: Pairs of MI images and Ground Truth (GT) shadow masks were prepared for cGAN learning. Four MI images (approximately 3000 × 1200 pixels) are chosen at a high-latitude region, which had low solar elevation angles, because these images comprise many shadow regions. GT shadow masks are binary images, wherein 1 and 0 represent the shadow non-shadow regions, respectively. The GT shadow masks were generated by determining the thresholds for each MI image and modifying the masks manually. The accuracy of the shadow masks predicted using cGAN was affected by the accuracy of the GT shadow masks. Therefore, the GT shadow regions are excessively selected to decrease under-detection for the predicted shadow masks.

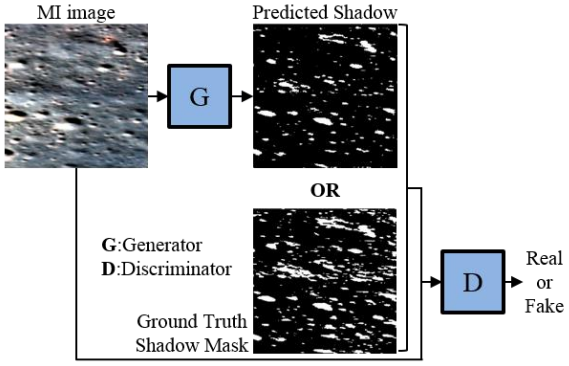

Figure 1: Structure of cGAN. White region represents a shadow region and black represents non-shadow region in GT and Predicted shadow masks, respectively.

Figure 1 shows the network structures of cGAN. The input data for the Generator is a patch cut out from the original size of MI images into 256 × 256 pixels, and the output is a predicted 256 × 256 shadow mask corresponding to the input data. The MI image has nine bands, and all bands are input into cGAN. The final layer (output function) of the Generator is softmax; therefore, the predicted shadow mask has a probability distribution of whether a given pixel is a shadow. The input data for the Discriminator is a pair of an MI patch and a GT shadow mask patch or an MI patch and predicted shadow mask patch (the patch size is 256 × 256 pixels). The Discriminator predicts whether the pair is real or fake.

We prepared 500 and 172 pairs of MI and GT shadow mask patches for cGAN training, and valida-

tion, respectively. The training dataset includes rotated patches for data augmentation. An epoch is the training cycle that includes all training data, and our approach is trained for 200 epochs.

Results: For testing, two regions, which include Anderson-E and F areas, were chosen because Anderson-E and F have relatively small DMDs (the areas of Anderson-E and F are approximately 81 and 31 km^2, respectively) [3]. Predicted shadow masks were generated using the trained Generator model. In the testing, 256 × 256 patches of the original MI image sampled with stride 128 pixels are prepared. In the overlapped area, the average probability is calculated. The shadow detection results corresponding to the original MI image form a binary image (threshold 0.5) with 1 and 0 for shadow and non-shadow regions, respectively. After this shadow detection, we would pick up the DMDs as the darkest region in the image.

Figure 2 shows the results of shadow detection and DMD detection in Anderson-E (left column) and F (right column) areas. In the results of shadow detection in these two regions, most of the shadow regions were detected (Figure 2(B)). Red areas in Figure 2C corresponds to the area with the reflectance smaller than 0.115. Around Anderson-E, many shadow regions were misclassified as DMDs (Figure 2(C)), whereas in the results from the shadow masked MI image, these shadow regions were removed (Figure 2(D)). However, in the results for Anderson-F (Figure 2, right column), DMD were not detected because almost all DMDs were detected as shadow regions.

Discussion and Conclusion: Based on these results, it is conceivable that the shadow detection methods using cGAN are useful for detecting DMDs with the sizes typical of the Anderson-E area from the shadow masked MI image. However, the DMDs with the size typical of the Anderson-F could be missed. The influence of the GT shadow masks is an origin of this difference. In this study, we excessively detected the shadow regions for the GT shadow masks. It is likely that the training dataset included shadow regions, which have similar size and shape to the Anderson-F sized DMDs. Additionally, for decreasing over-detection, the threshold for detecting DMDs was set to a relatively low value. If the threshold higher than 0.155 is used, around Anderson-F regions are detected as DMD, but the shadow regions that were not removed by the shadow masks are misclassified as DMDs. Thus, appropriate adjustment of the threshold is necessary.

Furthermore, the training dataset was generated merely from the four MI images obtained at the high-latitude region. Therefore, the variety of the shadow patterns is limited. While applying this method to the global lunar surface, this limitation will cause over- or under-detection of DMDs. For the accurate detection of the shadows, which have various sizes or shapes, and for the detection of smaller DMDs, modifying and increasing the GT shadow masks and improving the network structure of would be necessary.

Acknowledgement: This study is based on the results obtained from a project commissioned by the New Energy and Industrial Technology Development Organization (NEDO).

References: [1] Ohtake, M. et al. (2008) Earth, Planets and Space, 60(4), 257-264. [2] JAXA, "SELENE data Archive," http://darts.isas.jaxa.jp/planet/pdap/selene/index.html (accessed July 5, 2018). [3] Goodfellow, I. et al. (2014) Neural Information Processing Systems, 2672–2680. [4] Isola, P. et al. (2016) arXiv preprint arXiv:1611.07004. [5] Gustafson, J. O. et al. (2012) Journal of Geophysical Research: Planets, 117 E00H25.

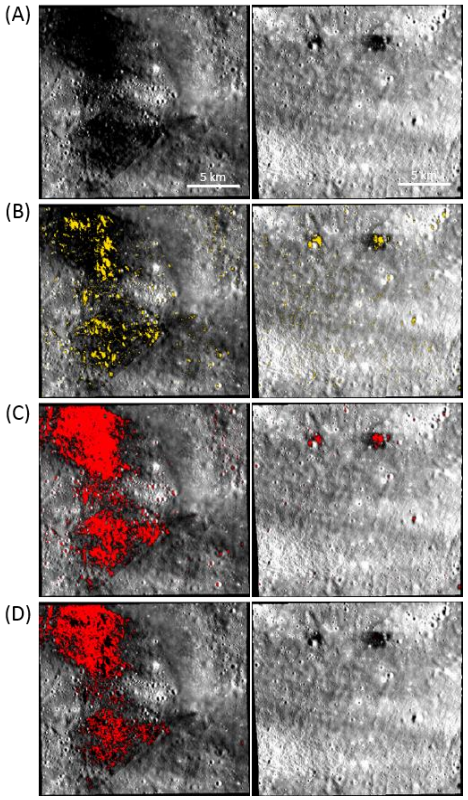

Figure 2: Results of shadow detection and DMD (Anderson-E: MIA_3C5_AA_03695N169E1738SC, Anderson-F: MIA_3C5_AA_03695N158E1738SC). The left and right columns show column respectively shows Anderson-E and F results. (A) Original MI images; (B), (C), and (D) respectively indicate results of shadow detection by cGAN (yellow is detected shadows), DMD detection via simple thresholding from original MI images, and DMD detection after shadow removal via cGAN (red is detected DMDs).